



Investigating Isotropy of Mechanical and Wear Properties in As-Deposited and Inter-Layer Cold Worked Specimens Manufactured by Wire Arc Additive Manufacturing

Behzad Parvaresh¹ · Reza Salehan¹ · Reza Miresmaeili¹

Received: 15 April 2020 / Accepted: 15 June 2020 / Published online: 2 July 2020
© The Korean Institute of Metals and Materials 2020

Abstract

Wire arc additive manufacturing (WAAM) has several industrial applications because of its advantages over other additive manufacturing methods. In this study, two stainless steel 347 walls, namely as-deposited (AD) wall, and inter-layer cold worked (CW) wall, were prepared using the WAAM method to investigate the isotropy of their mechanical properties and wear properties in vertical and horizontal directions. For the AD wall, the mean yield strength, ultimate strength, and elongation of horizontal samples were 410 MPa, 620 MPa, and 47%, respectively. In comparison, these values for the vertical (V) samples were 402 MPa, 590 MPa, and 49%, respectively. For the CW wall, the mean yield strength, ultimate strength, and elongation of horizontal samples were 815 MPa, 876 MPa, and 26%, respectively, while those of vertical samples were 722 MPa, 824 MPa, and 25%, respectively. The CW wall's tensile test results indicated that inter-layer cold working intensified the anisotropy of tensile properties in both vertical and horizontal directions. Microstructural investigation revealed that inter-layer cold working and the heat resulted from subsequent layers deposition in the CW wall recrystallized the layers and reduced the grain size. Additionally, wear test results demonstrated that inter-layer cold working increased hardness and thus wear-resistance of the samples and reduced their friction. The results showed that the coefficient of friction (COF) and wear rates of the samples are not highly dependent on their direction.

Keywords Wire arc additive manufacturing · Anisotropy · Mechanical properties · Wear properties · Microstructure

1 Introduction

Additive manufacturing (AM) technology has received much attention in industry and academic settings in recent decades [1]. AM is a process in which components are manufactured layer upon layer based on a 3-dimensional model [2]. This method is cost and time saving and allows the manufacturing of pieces with complex geometry [3]. Ebrahimi et al. [4] reported that various energy sources are used in the AM process, such as electric arc, laser rays, and electron rays,

and the utilized raw materials may be powders or metal wire, depending on the process type.

One of the AM processes is wire arc additive manufacturing (WAAM) method that has advantages such as a high deposition rate. This process is employed to manufacture pieces in relatively large dimensions with medium geometric complexity [5]. According to Honnige et al. [6], the disadvantages of this method are distortion due to high heat input during layer deposition, high residual stress, welding defects, poor dimensional precision, and lower surface quality than other AM methods.

Among recent studies conducted on WAAM, Colegrove et al. [7] explored the effects of inter-layer cold working on Al and Ti alloy pieces manufactured by the WAAM method. They reported that inter-layer rolling reduced porosity in the aluminum sample and increased its flexibility. Furthermore, inter-layer cold working miniaturized and equiaxed initial β grains in the titanium sample. In another study, Xu et al. [8] investigated the effects of thermomechanical processes on INCONEL 718 Super Alloy samples manufactured by

✉ Reza Miresmaeili
miresmaeili@modares.ac.ir

Behzad Parvaresh
b.parvaresh@modares.ac.ir

Reza Salehan
rz.salehan@modares.ac.ir

¹ Department of Materials Engineering, Tarbiat Modares University, Tehran, P.O. Box: 14115-143, Iran

the WAAM method. According to their results, as-deposited samples had lower tensile properties after heat treatment than the wrought ones. At the same time, inter-layer cold working in other samples resulted in non-uniform recrystallization and compared to the wrought mode, their ultimate strengths enhanced after heat treatment.

Guo et al. [9] produced an AZ80M magnesium alloy wall by the WAAM method and studied its tensile properties in both horizontal and vertical directions. The results revealed that the horizontal samples had higher tensile properties than vertical ones because of their heterogeneous microstructures and the aggregation of cracks in inter-layer areas. Studying WAAM bainite steel samples, Fu et al. [10] found that AD samples had anisotropic tensile properties in three building directions of X, Y, and Z. They showed that inter-layer cold working provided more isotropic tensile properties in three building directions and the fracture toughness of these samples became three times larger than that of AD ones. Wu et al. [11] reported that the cooling rate of layers increased as the heat input reduced during manufacturing Ti-6Al-4V components by the WAAM method. Moreover, they reported that the high cooling rate of layers increased tensile properties such as yield strength and ultimate strength. Xie et al. [12] reported that WAAM 1045 steel AD samples had anisotropic tensile properties in vertical and horizontal directions. Inter-layer cold working improved the tensile properties in both vertical and horizontal directions; however, there was still anisotropy in the properties in two directions.

Attar et al. [13] suggested that parameters such as material feeding system and energy resource may affect the melting, solidification, and microstructures of AM pieces, thereby influencing their mechanical and wear properties. Yang et al. [14] studied the effects of the wear force on the isotropic and anisotropic wear behavior of 316 L stainless steel samples manufactured by the Selective Laser Melting (SLM) method. They showed that wear properties were dependent on the building direction at low forces (1 and 3 N) while the building direction did not significantly affect the wear properties at high forces (5 N). Marenych et al. [15] manufactured FM60 and Monel K500 samples using the WAAM method to investigate the effects of manufacturing speed on the mechanical properties and wear properties. The results demonstrated that the Monel K500 samples had higher mechanical and wear properties than the FM 60 samples, and samples manufactured at 400 mm/min had the highest toughness and thus the wear resistance.

Among studies conducted on AM components, there are a limited number of works on wear behavior, mechanical properties, and the isotropy of properties in different directions. Moreover, most of the studies in this context have explored Al and Ti alloys, while a low number of them have investigated steel pieces. In the present study, AD and CW stainless steel 347 walls were prepared using the WAAM

method. Then, tensile tests and the pin-on-disk wear tests were performed to study the effects of inter-layer cold working and isotropy of mechanical and wear properties in vertical and horizontal directions. Finally, the microstructures of the samples were examined to discuss the mechanical and wear tests' results.

2 Experimental

2.1 Sample Preparation

The walls were built using stainless steel 410 substrates with dimensions of 260 mm × 60 mm × 40 mm. A Fronius Cold Metal Transfer (CMT) welding resource with an average travel speed of 7 mm/s was used to build the layers. The wire feed speed in the process, according to multiple pretests, was set 0.4 m/min with a current and voltage of 135 A and 11.8 V, respectively. A shielding gas containing 97.5% of Ar and 2.5% of CO₂ was used in this process. The welding wire was made of stainless steel 347 with 1.2 mm of diameter. In this study, two walls, namely as-deposited (AD) wall, and inter-layer cold worked (CW) wall, were built to examine the effect of inter-layer cold working on mechanical properties and wear properties. Five layers were deposited on the substrate at the beginning and then removed from the main wall by machining after the wall was built entirely in order to make approximately similar dilution and cooling rate for all subsequent layers. Time is a factor which is important in manufacturing products with AM method. After depositing each layer, it takes a long time to cool down to the room temperature. So the maximum temperature (150 °C) close to the cold work temperature was specified. Moreover, a thermometer was used for measuring each layer's temperature. Also, after depositing each layer, the next layer's deposition was not started unless the previous layer's temperature dropped below 150°C. The AD wall was built with 240, 8.5, and 124 mm of length, width, and height, respectively, without inter-layer cold working (Fig. 1). The CW wall was built in the same manner except that once each layer was deposited, its temperature was decreased below 150°C, and then it was deformed under 350 bars of pressure, followed by depositing the subsequent layer on the previous cold-worked layer. All the layers in the CW wall were built on each other using the mentioned process. Also, a manually operated hydraulic press was utilized to deform the layers.

2.2 Tensile test

To investigate the effects of cold working on the walls' mechanical properties and isotropy of tensile properties in vertical and horizontal directions, both AD and CW walls

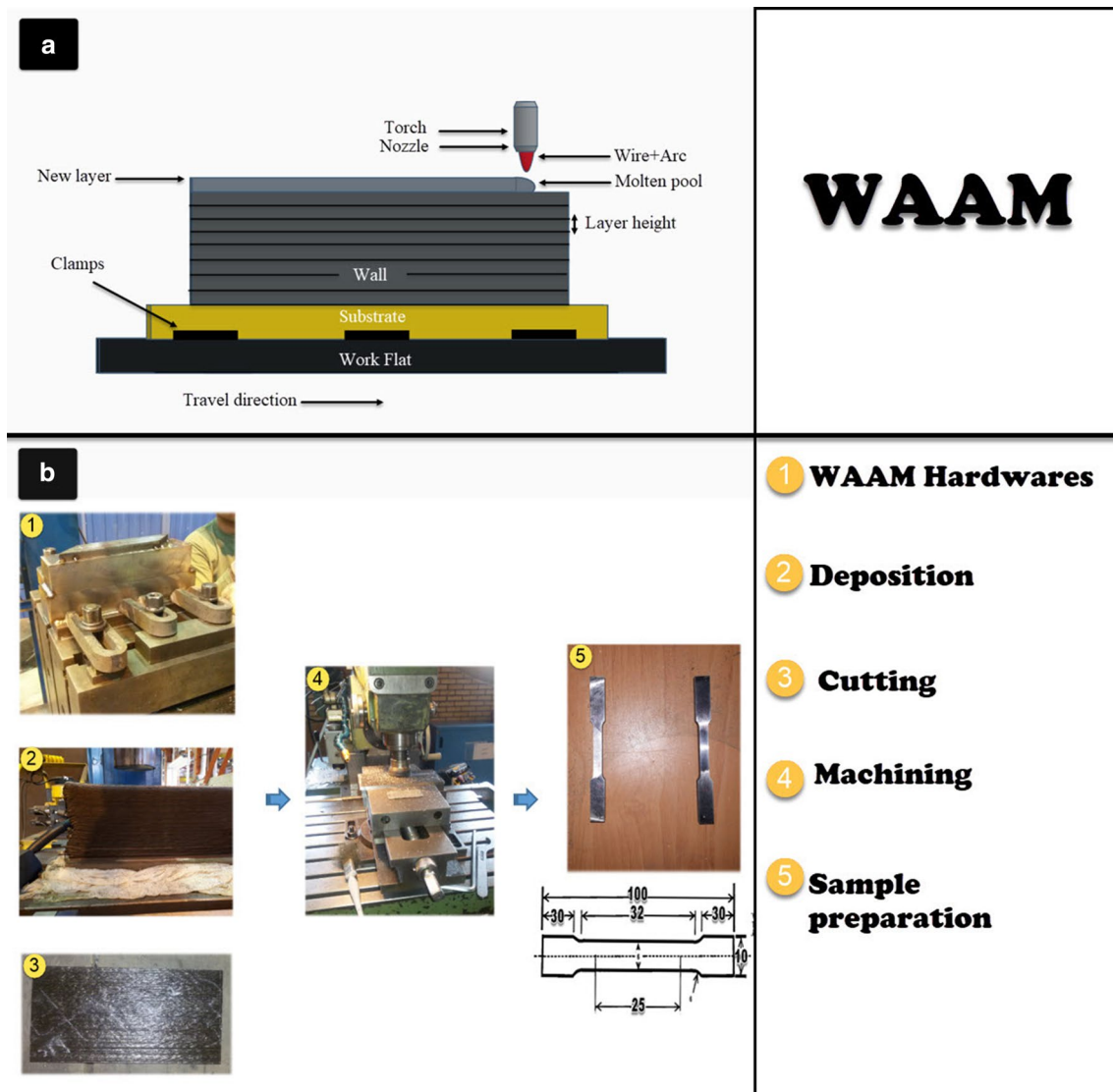


Fig. 1 a The schematic of WAAM b Building stages of AD and CW samples

were machined in the same dimensions. Then, the tensile test samples were prepared in accordance with the process described in the following. As can be seen in Fig. 2a, vertical (V) and horizontal (H) tensile test samples were extracted from the top (H_T), middle (H_M), and bottom (H_B) of the walls in the determined areas. For the repeatability of the tensile test results, three tensile samples were taken from each of the mentioned areas (V, H_T , H_M , H_B). The tensile samples were prepared in the dimensions of 100 mm \times 10 mm \times 6 mm according to ASTM E 8M standard. All the tensile tests were carried out at room temperature with the strain rate of 0.15 mm/mm/min. Table 1 presents the specifications of the tensile and wear samples.

2.3 Microstructural Analysis

The samples for microstructural investigation were cut from the middle of the AD and CW walls, perpendicular to the layers. Then, they were polished and etched in an electrolyte solution containing 40 ml H_2O and 60 ml HNO_3 at a voltage of 1.1 V for 120 s. The samples were characterized using optical microscopy (OM) and the scanning electron microscopy (SEM).

2.4 Wear Test

As can be seen in Fig. 2b, vertical (V) and horizontal (H) wear test samples were extracted from both AD and CW walls. The pin-on-disk wear tests were carried out at the ambient temperature in dry sliding conditions, in accordance

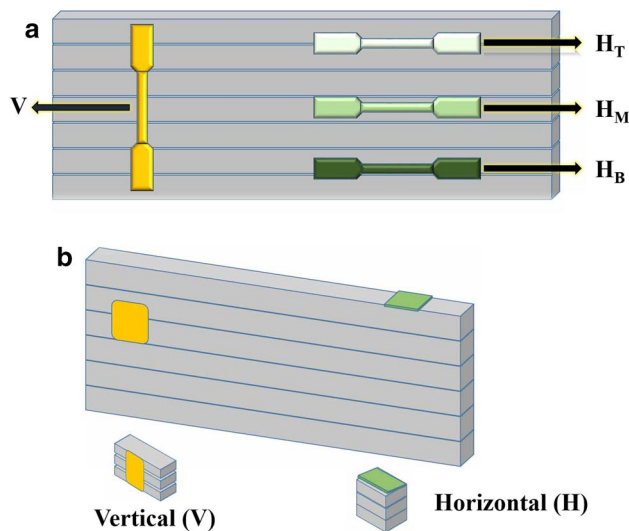


Fig. 2 Extraction areas of horizontal and vertical **a** wear samples **b** tensile samples

with ASTM-G99-05 standard [16]. Before the test, the entire surface of the samples was prepared by emery cloths No. 80 to 2000 and polished using a 0.3 μm Alumina solution. The samples were ultrasonically washed in an alcohol-acetone solution before and after the test. Next, they were weighed using the A&D scale N92 with an accuracy of 0.1 mg. The density of the samples was measured by the Archimedes' principle. For the wear test, an AISI 52100 bearing steel pin with 15 mm of diameter was utilized. The wear test was performed with two forces of 5 and 10 N at a linear velocity, wear track diameter, rotational sliding velocity, and the total distance of 0.05 mm/s, 4.5 mm, 212 rpm, and 500 m, respectively. Each wear test was performed in triplicate, and the mean coefficient of friction (COF) and wear rate were recorded. The sample's worn surfaces were investigated using SEM.

Table 1 Specifications of tensile and wear samples

Specimen	Wall	Direction	Region	Test
H_T	Cold worked, AS deposited	Horizontal	Top	Tensile test
H_M	Cold worked, AS deposited	Horizontal	Middle	Tensile test
H_B	Cold worked, AS deposited	Horizontal	Bottom	Tensile test
V	Cold worked, AS deposited	Vertical	–	Tensile test
V_{AD}	AS deposited	Vertical	Middle	Wear test
H_{AD}	AS deposited	Horizontal	Middle	Wear test
V_{CW}	Cold worked	Vertical	Middle	Wear test
H_{CW}	Cold worked	Horizontal	Middle	Wear test

2.5 Microhardness Test

To determine the hardness of wear samples' surface, they were all polished, and the microhardness test was carried out with a Vickers indenter at 30 g of load for 15 s using the MICROMET BUEHLER ILLINOIS-60044 machine. All tests were taken according to the ASTM E384-99 standard [17].

3 Results and Discussion

3.1 Tensile Test

Tensile test results for the AD and CW walls are presented in Fig. 3. As can be seen, for the AD wall, the mean yield strength, ultimate strength, and elongation of horizontal samples (H_T , H_M , and H_B) are 410 MPa, 620 MPa, and 47%, respectively, while those of the vertical (V) samples are 402 MPa, 590 MPa, and 49%, respectively. Moreover, in the CW wall, the mean yield strength, ultimate strength, and elongation of horizontal samples (H_T , H_M , and H_B) are 851 MPa, 876 MPa, and 26%, respectively, while those of the vertical (V) samples are 722 MPa, 824 MPa, and 25%, respectively. However, the strain rate reported in this study for tensile tests is slightly higher than the usual strain rate for reporting yield strength and elongation.

The minimum yield strength, ultimate strength, and elongation stated in the ASTM-A240 standard [18] for stainless steel 304 plates are 205 MPa, 515 MPa, and 40%, respectively, which are in line with the tensile properties of the AD wall. As also reported by Tan et al. [2], the AD steel samples built by the SLM method had the minimum standard values. Elsewhere, in a study conducted by The International Nickel Company [19], the yield strength of stainless steel 304 increased to 896 MPa due to cold working.

Comparing the tensile properties of H_B , H_M , and H_T samples extracted from the top, middle, and bottom of the AD wall reveals that mechanical properties are almost uniform across the wall, and they do not depend on the extraction location. Elsewhere, Haden et al. [20] studied WAAM stainless steel 304 samples and proposed the tensile properties of different locations of an AD wall to be different and dependent on the extraction location.

Furthermore, the comparison of the tensile properties of horizontal samples (H_B , H_M , and H_T) to those of the vertical samples of the AD wall shows apparent isotropy, suggesting that the tensile properties of the AD wall are not dependent on the horizontal and vertical directions of the samples. This result is consistent with those of Gu et al. [21] and Qi et al. [22]. However, this apparent isotropy between as-deposited horizontal and vertical samples is not seen in the work of

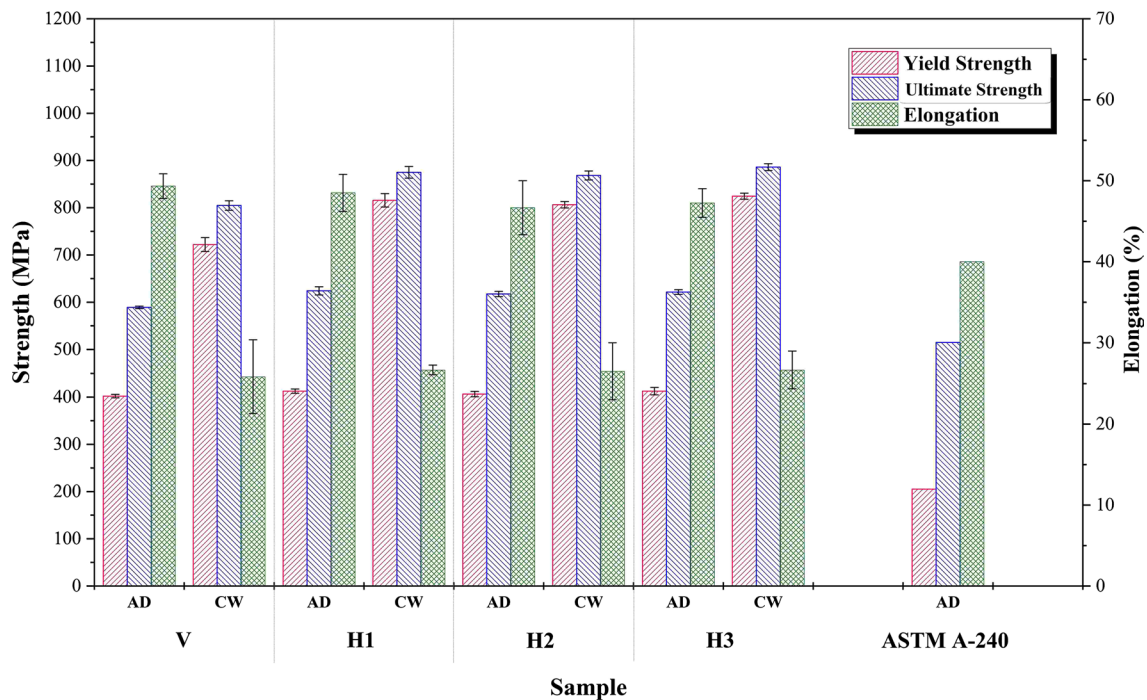


Fig. 3 Tensile test results of AD and CW walls in horizontal and vertical directions. Error bars represent standard deviation of three tensile tests of each area

Guo et al. [9], who studied magnesium alloy samples, and Fu et al. [10], who investigated WAAM bainite steel samples.

Comparing the tensile results of the AD and CW walls demonstrates that inter-layer cold working increased the yield strength and ultimate strength and reduced the elongation. In a similar study, Gu et al. [23] reported that yield strength and ultimate strength increased with an increase in the amount of inter-layer cold working for WAAM samples.

Comparing the tensile properties of H_T , H_M , and H_B extracted from the top, middle, and bottom of the CW wall shows that the tensile properties are uniform across the CW wall and are independent of the sample extraction location. Additionally, comparing the tensile results of horizontal samples (H_B , H_M , and H_T) with those of the vertical (V) samples in the CW wall indicates that inter-layer cold working intensified the apparent anisotropy of horizontal and vertical samples' tensile properties. In comparison to the AD wall, inter-layer cold working changed the difference in the mean yield strength between horizontal and vertical directions from 8 to 93 MPa and the mean ultimate strength from 30 to 52 MPa. In a study by Xu et al. [8] on INCONEL 718, inter-layer rolling changed the difference in the mean yield strength between horizontal and vertical directions from 19 to 76 MPa and the mean ultimate strength from 62 to 10 MPa. In a study by Xie et al. [12] conducted on stainless steel 304, inter-layer rolling did not provide isotropic tensile properties in horizontal and vertical directions. At the same

time, in Fu et al. [10] and Martina et al. [24], inter-layer cold working provided isotropic tensile properties in horizontal and vertical directions. Overall, in this study, tensile properties of the CW wall were dependent on the horizontal and vertical directions of the samples, but not the sample extraction locations.

The microstructures of the AD and CW walls were investigated to explore the causes of anisotropic tensile properties between horizontal and vertical directions due to inter-layer cold working. Studying the microstructure of the AD wall (Fig. 4a, b) revealed that the layer's solidification microstructure was composed of columnar dendrites of austenite, vermicular ferrite, and lathy ferrite. This observation was reported in Inoue et al. [25, 26], Elmer et al. [27], Yilmaz et al. [28], and Kotecki et al. [29], as well.

Since layers are built on each other in the WAAM method, the heat resulting from depositing each layer changes the temperatures of the previously built layers. Microstructural investigation of the AD wall's layers shows that the heat cycle induced by the subsequent layers' deposition did not significantly affect the previously built layers' microstructural evolution. At the same time, it is seen in Fig. 4c, d, e (of the CW wall) that inter-layer cold working and the heat due to the deposition of the subsequent layers evolved the microstructure of previously built layers. Through this microstructural evolution, austenite column dendrites recrystallized during the CW

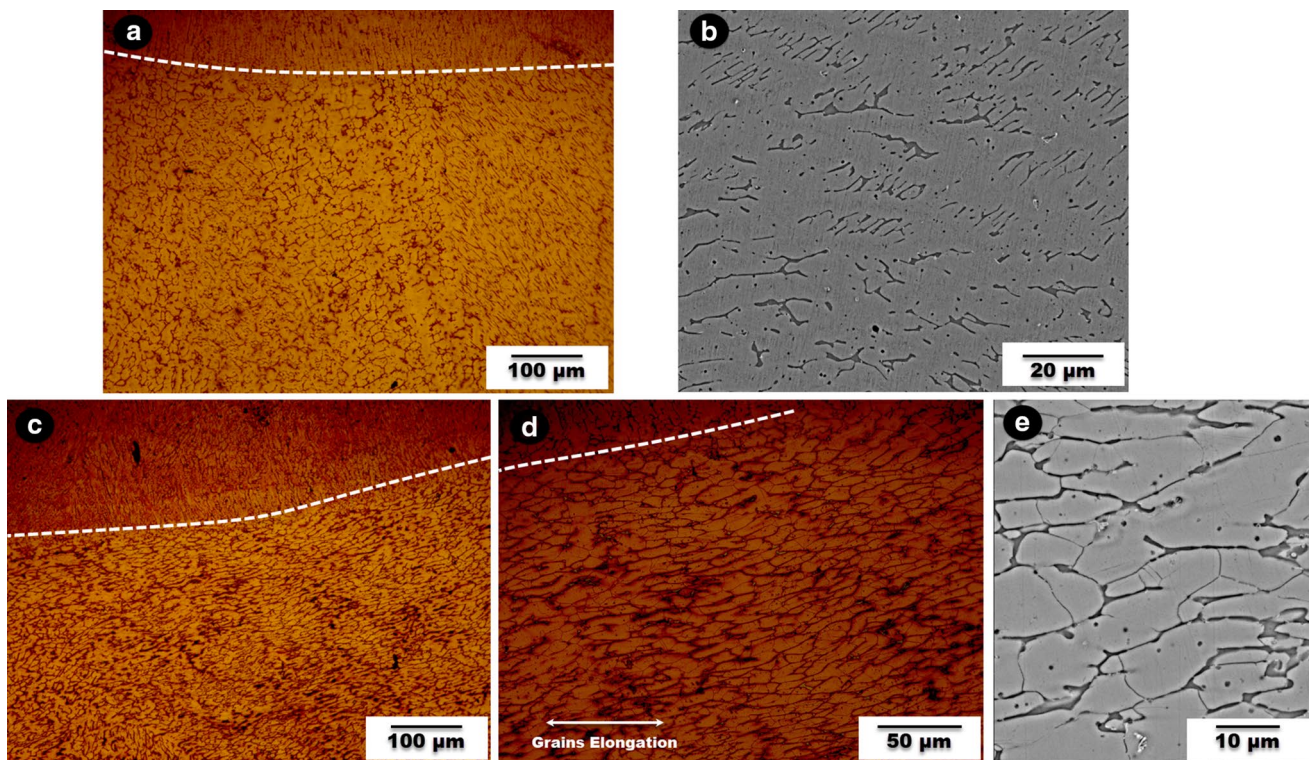


Fig. 4 (a, b) AD wall layers' microstructure; (c, d, e) CW wall microstructure

walls' building process in the areas near to the layer surface and the grain sizes decreased. In a similar study, Colegrove et al. [7] transformed initial β grains of Ti-6Al-4V alloy microstructure into fine equiaxed grains during the WAAM process by interlayer rolling. Moreover, Xu et al. [8] applied inter-layer rolling during the WAAM process and transformed solidified INCONEL 718 microstructure with large column grains into a non-homogenous microstructure consisting of a recrystallized core with fine equiaxed grains and small column grains.

The recrystallized equiaxed grains of the previous layers were deformed and elongated by the cold working of the subsequent layers in the process of manufacturing the CW wall (Fig. 4d, e). This circumstance can provide better tensile properties in the horizontal direction than the vertical direction in the CW wall and be the cause of anisotropic tensile properties in horizontal and vertical directions. Studying the effects of rolling on dual-phase steel's tensile properties, Ahmad et al. [30] suggested that rolling enhanced the anisotropy of ultimate strength and slightly changed the steel samples' elongation. They also demonstrated that the strength of the rolled steels is higher in the longitudinal direction than in the transverse direction. Elsewhere, in a study conducted by Fu et al. [10] on WAAM bainite steel samples, inter-layer rolling transformed the column dendrite structure into equiaxed grains and eliminated the anisotropy of the tensile

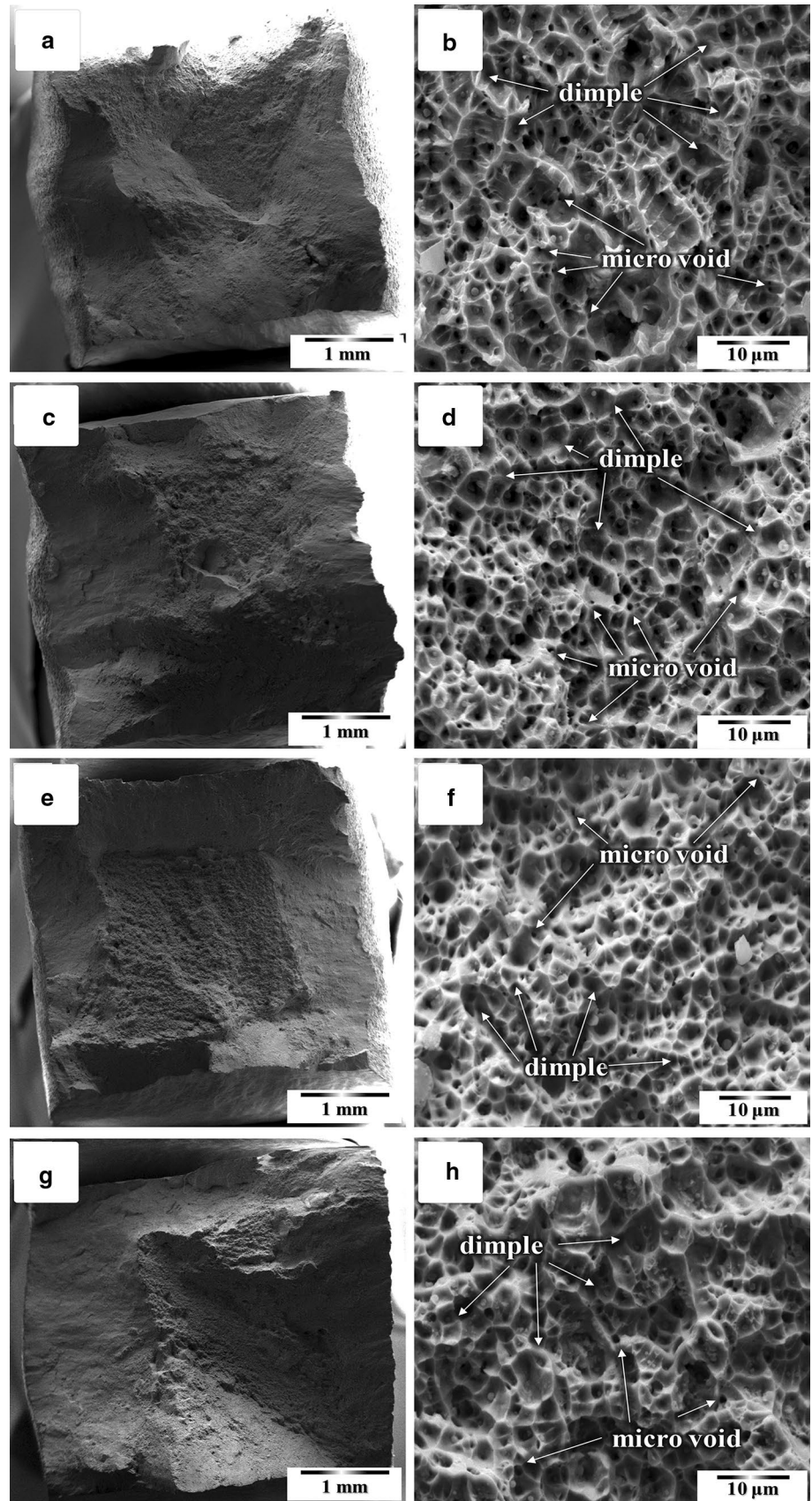
properties. Also, it significantly improved the samples' tensile properties and fracture toughness.

3.2 Microscopic Fracture Behavior

Tensile samples V and H_M were selected to investigate the AD and CW wall's fracture surfaces. Figure 5a, c, e, and g illustrate the SEM images of the samples' fracture surfaces fractography at low magnification, while Fig. 5b, d and f, indicate the same surfaces at the high magnification.

Comparing the fracture surfaces at low magnification indicates that the fracture surfaces of samples H_M and V of the AD wall (Fig. 5a, c) underwent a high plastic deformation. Moreover, the results show regions of micro-void coalescence for those samples. At the same time, in samples H_M and V of the CW wall (Fig. 5e, g), the smooth surface ratio to the total fracture surface increased, so it shows higher brittleness and lower plastic deformation. The images at higher magnification demonstrate that all the four fracture surfaces have dimples, suggesting the presence of a ductile fracture [11, 21, 31]. Ductile fracture surfaces typically have a fiber appearance with deep dimples [32]. Indeed, the dimples of each sample are different in size because of different building processes. Broad and deep dimples are observed in the fracture images of the AD wall (Fig. 5b, d), indicating ductile fracture and high flexibility. In the images of the CW

Fig. 5 SEM fractography for tensile samples **(a, b)** H_M sample of AD wall **(c, d)** V sample of AD wall **(e, f)** H_M sample of CW wall **(g, h)** V sample of CW wall



wall (Fig. 5f, h), due to inter-layer cold working and reduced flexibility, the dimples are smaller and shallower, and the fracture is more brittle than the AD wall. The formation of fine and numerous dimples on ductile metals' fracture surfaces indicates their high strengths resulting from the nucleation of a high number of microvoids during considerable strains [23].

3.3 Tribological Behavior

Figure 6a depicts COFs obtained from the wear samples of the AD and CW walls in horizontal and vertical directions. The results indicate that the samples' COFs were in the range of 0.16–0.25 and 0.24–0.36 at loads 5 and 10 N, respectively. So, it can be stated that an increase in the load of the wear test increased the COFs of the studied samples. Yang et al. [14] reported that wear force considerably affected the samples' wear properties in different building directions and the increased COF due to increased load for wear of the stainless steel was reported in [33, 34], as well. Furthermore, the same COF of samples V_{AD} and H_{AD} and

the same COF of V_{CW} and H_{CW} at both loads indicate that COF and tribological behavior are independent of vertical and horizontal directions.

Figure 6b compares the wear rates of samples V_{AD} and H_{AD} and those of samples V_{CW} and H_{CW} at load 5 and 10 N. Unlike results reported by Haden et al. [20], the wear rate is not a function of the sample extraction location of the built walls and deposition direction. In a similar study, Li et al. [35] investigated selective laser melted 316 L stainless steel and reported that samples' directions did not significantly affect the wear rates and COFs of the samples. Additionally, comparing the results of AD and CW samples suggests that cold working reduced wear and COF.

Figure 7 shows the mean microhardness of the wear samples' surfaces. The same hardness of samples V_{AD} (256 ± 2 HV) and H_{AD} (250 ± 5 HV) represents the isotropy of mechanical properties. Yang et al. [14] and Li et al. [35] investigated selective laser melting (SLM) 316 L stainless steel components and reported the same hardness for the faces of the prepared samples.

Inter-layer cold working compared to AD samples increased the hardness by 34% and 38% in the vertical direction and horizontal direction, respectively. In this regard, Gu et al. [21] reported similar results. Furthermore, they reported that cold working increased the hardness uniformity in the direction perpendicular to the layers. In the previous section, it was observed that cold working increased the anisotropy of the tensile results; however, no cold working-induced increase is seen in the hardness anisotropy of the samples in Fig. 7.

Figures 8 and 9 represent the worn surfaces of wear samples of the AD and CW walls in horizontal and vertical directions at loads of 5 and 10 N, respectively. The worn surfaces show similar appearances because the activated mechanisms of the samples' wear are the same [34]. In the other hand increasing the load from 5 to 10 N did not cause

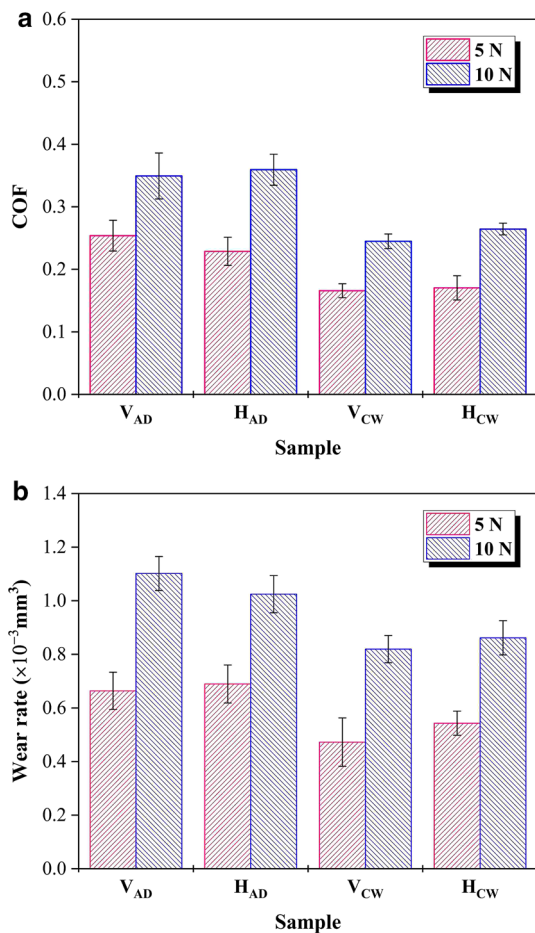


Fig. 6 a Mean coefficient of friction at steady-state and b wear rates

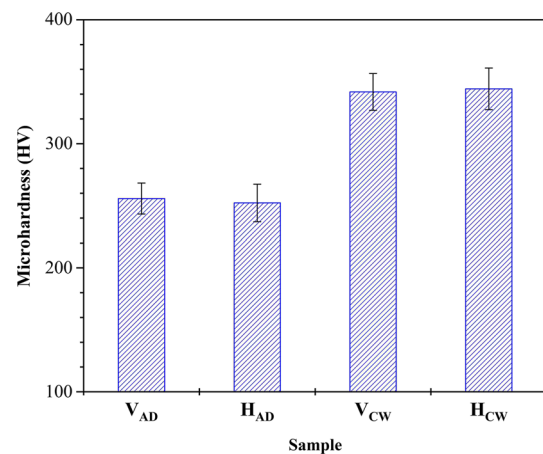


Fig. 7 Microhardness of the studied samples

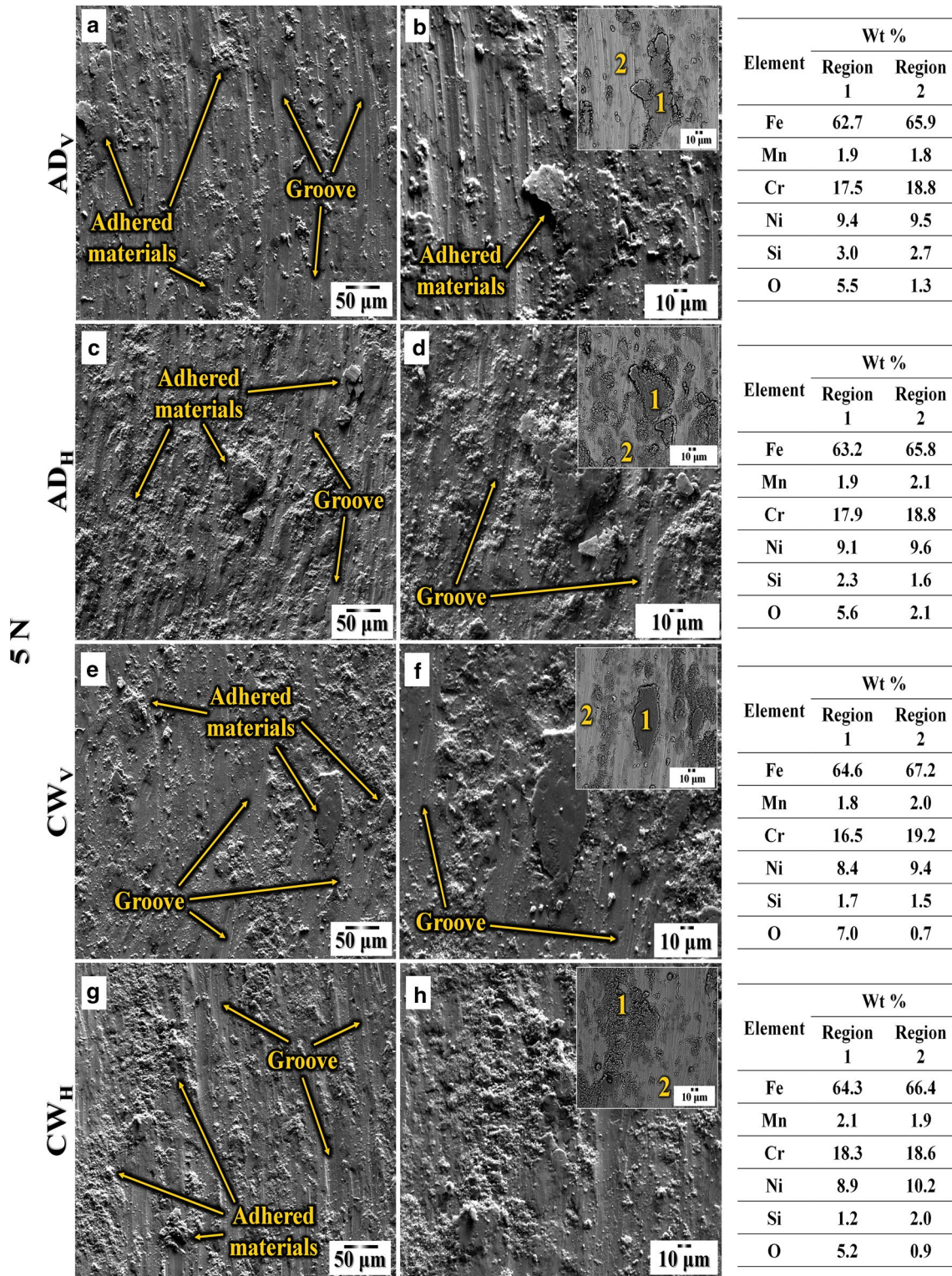


Fig. 8 Worn surfaces of the As deposited samples in (a, b) vertical and (c, d) horizontal directions, and cold worked samples (e, f) vertical and (g, h) horizontal directions at a load of 5 N and secondary

electron mode; insets are at backscattered electron mode, and the table contains the EDS results of the numbered locations

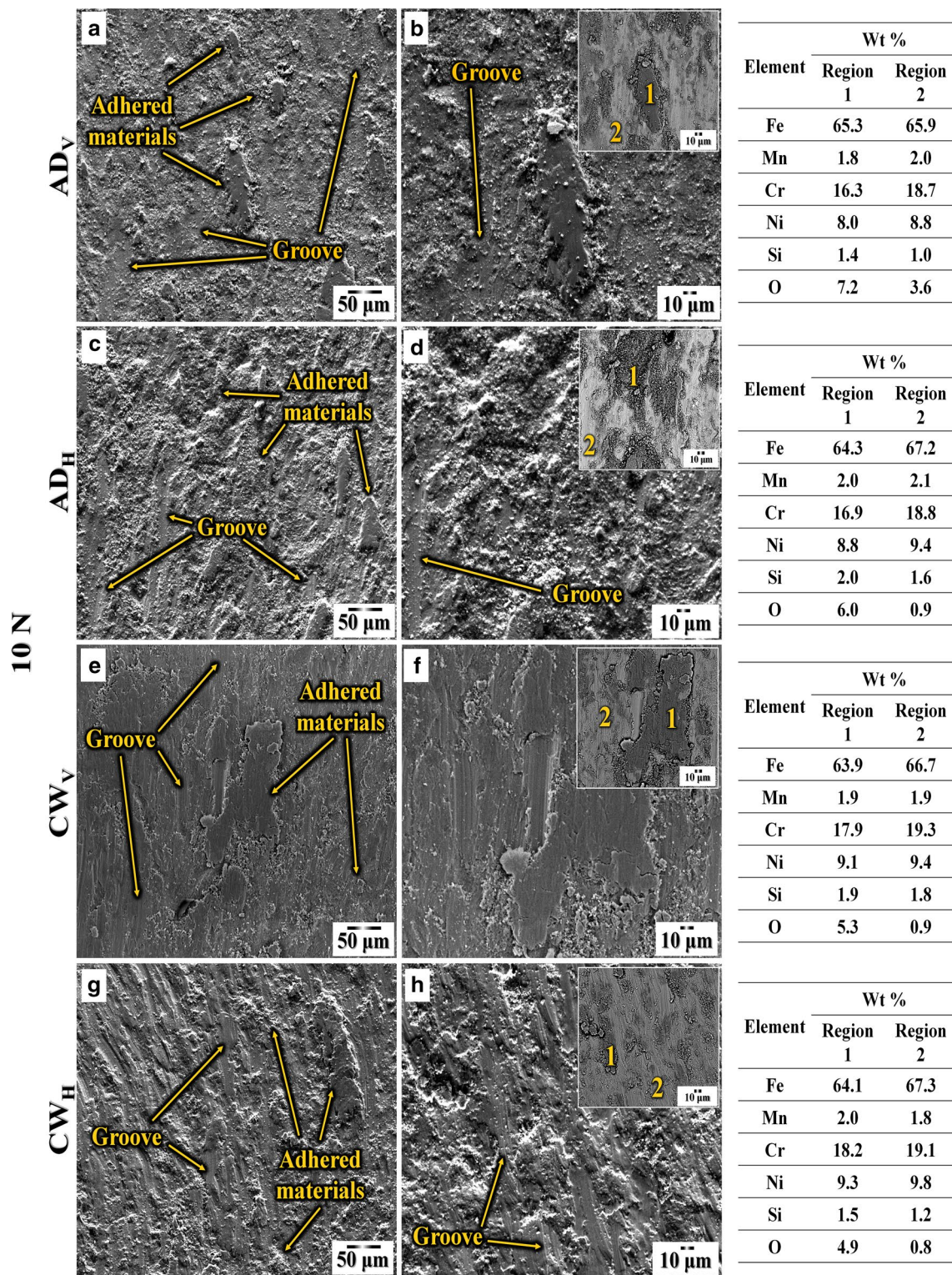


Fig. 9 Worn surfaces of the As deposited samples in (a, b) vertical and (c, d) horizontal directions, and cold worked samples (e, f) vertical and (g, h) horizontal directions at a load of 10 N and second-

ary electron mode; insets are at backscattered electron mode, and the table contains the EDS results of the numbered locations

a significant change in wear features and the nature of the activated mechanisms, which discusses the nature of these activated mechanisms, in the next paragraph.

The EDS results in Figs. 8 and 9 represent that the chemical composition of the areas on the worn surfaces are almost the same, and only the oxygen content considerably increased in the particles on the surface (indicated as areas No. 1) compared to the other areas. Distribution of the particles of different sizes containing considerable amounts of oxygen in their chemical compositions supports the dominance of adhesion wear mechanism in the samples' wear [33, 34]. The surface oxidation and wear debris also were reported on stainless steel wear [33]. Other investigations show long parallel grooves in the direction of wear on some worn surfaces, implying the activation of abrasion wear mechanism in the samples' wear [35, 36]. In recent studies, the simultaneous activation of both abrasion and mixed-mode wear mechanisms were reported for stainless

steel wear [33]. These surface properties were observed in AM metal wear [13][36][37].

Figure 10 illustrates the mean wear track widths of the samples. In line with the study of Rai et al. [33], it is seen that an increase in the load increased the wear track width. Moreover, it is seen that the AD wear track width is higher than that of the CW wear track width at both loads of 5 and 10 N. Table 2 summarizes the wear test findings.

According to Archard's equation, materials' wear resistance has a linear relationship with their hardness [13, 38]. In this regard, several studies have reported the effect of ductility on wear resistance [15, 39]. Considering hardness results (Fig. 7) and tensile results (Fig. 3), the hardness and elongation of the vertical sample (V) did not considerably differ from that of the horizontal sample (H) in AD mode. The similarity of the hardness and elongation values in vertical and horizontal samples has caused the wear resistance and COF of samples V_{AD} and H_{AD} to be the same. This is also true for samples V_{CW} and H_{CW} .

Moreover, Li et al. [35] reported that the building direction did not significantly influence COF and wear rate. At the same time, a relatively high wear force (e.g., 5 and 10 N) increases compressive stress and thus wear. The compressive stress induces plastic deformation and destruction of the oriented structure in subsurface layers [14]. Thus, the sample's wear behavior is not significantly dependent on their directions.

According to Fig. 10, the increased wear track width and load imply more intensive plastic deformation at 10 N than at 5 N, even though the same wear mechanisms were activated at loads of 5 and 10 N (Figs. 8, 9), which might have increased the wear rate. Rai et al. [33] and Li et al. [35] reported that more intensive plastic deformation increased the wear rate, despite activation of the same wear mechanisms.

Particles continue to separate from the surfaces of the pin and disk during wear such that rolling and mechanical

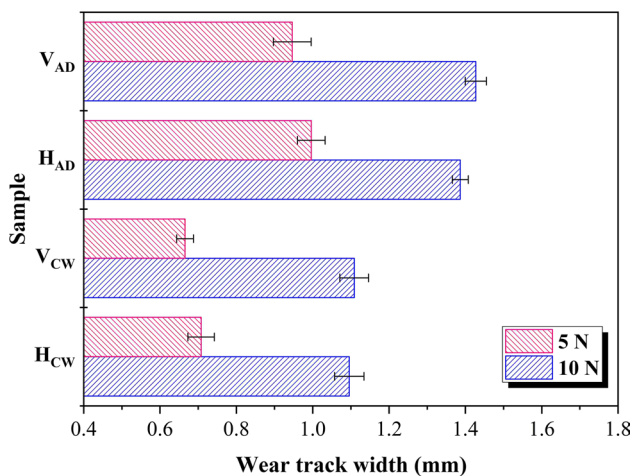


Fig. 10 Mean wear track width

Table 2 Summary of wear test results

Sample	H (HV)	COF		W (*10 ⁻³ mm ³)		Wear track width (mm)		Wear mechanism			
		5 N	10 N	5 N	10 N	5 N	10 N	5 N		10 N	
								Dominant	Other	Dominant	Other
V_{AD}	256 ±12	0.25 ±0.02	0.35 ±0.04	0.66 ±0.07	1.10 ±0.06	0.95 ±0.05	1.43 ±0.03	Adhesive	Abrasive	Adhesive	Abrasive
H_{AD}	250 ±15	0.23 ±0.02	0.36 ±0.03	0.69 ±0.07	1.02 ±0.07	0.99 ±0.04	1.38 ±0.02	Adhesive	Abrasive	Adhesive	Abrasive
V_{CW}	342 ±15	0.16±0.01	0.24 ±0.01	0.47 ±0.09	0.82 ±0.05	0.66 ±0.02	1.11 ±0.04	Adhesive	Abrasive	Adhesive	Abrasive
H_{CW}	344 ±17	0.17 ±0.02	0.26 ±0.01	0.54 ±0.04	0.86 ±0.06	0.71 ±0.03	1.09 ±0.04	Adhesive	Abrasive	Adhesive	Abrasive

alloy processes occur between surfaces. Wear debris rolling between surfaces, three-body wear activation [33], and the agglomeration and joining together of the debris [34] are among the factors affecting COF. More intensive plastic deformation at 10 N can make different morphologies and dimensions of the debris between 10 N-wear and 5 N-wear. This may change (increase) COF at 10 N from that at 5 N [33, 34].

The presence of oxygen in different areas (areas marked 1 in Figs. 8 and 9) on the worn surfaces suggests increased surface temperatures due to friction heating. Previous studies revealed that the steel surface temperature locally increased when the steel was worn by a steel counterpart [35, 38]. The surface oxidizes in exposure to the air oxygen due to the locally increased surface temperature during wear (air-exposed iron oxidizes because of high temperature). As shown in Figs. 8 and 9, the oxide layer is easily separated from the surface by the abrasion wear mechanism, and the fresh surface is exposed to the air oxygen. Because of the repetitive rotational movement of the pin-on-disk during wear, passive oxide layers on the surface are plowed and removed from the surface by the counterpart. In the other hand, dispersion of the adhered materials on the worn surface (Figs. 8b, d, e, h, 9b, d, e, h) illustrate that during the adhesive wear, the mechanical alloying continuously occurred, and its brittle products were removed from the surface. This process continues to repeat until the wear is completed [35]. At the CW mode, due to the work hardening after cold work and thus increased hardness (Fig. 7), the samples' wear resistance increased while their COFs reduced [40].

4 Conclusion

This study investigates as-deposited, and inter-layer cold worked WAAM stainless steel 347 walls to explore the effects of inter-layer cold working, the isotropy of mechanical properties, and wear properties in horizontal and vertical directions. The significant findings of this study can be outlined as follows:

- For the AD wall, the tensile properties were uniform across the wall and not dependent on the sample extraction location. Also, the tensile properties had apparent isotropy in horizontal and vertical directions.
- Inter-layer cold working enhanced the anisotropy of the CW wall's tensile properties in horizontal and vertical directions, but the tensile properties were uniform across the CW wall.
- Microstructural investigation showed that the heat cycles induced by the layers depositing on each other did not significantly change the microstructure of the AD wall's

layers. At the same time, inter-layer cold working and subsequent layer deposition heat of the CW wall non-uniformly recrystallized the layer surface-near areas, and thus the grain sizes were decreased in those areas.

- The closeness of the strength, elongation, and hardness values, in the samples in horizontal and vertical directions has caused the similarity of wear resistance and COFs values in both vertical and horizontal directions. Increasing the wear force from 5 to 10 N has increased the plastic deformation, resulting in increased COF and wear resistance. All of these are true for both cases AD and CW.
- The wear results of the pin-on-disk test showed that COF and wear rate were not considerably dependent on the direction (whether horizontal or vertical). Inter-layer cold working increased hardness and thus wear resistance and reduced COF. The dominant wear mechanism was the abrasion wear mechanism. An increase in the load resulted in greater wear track plastic deformation and thus higher wear rate and COF.

Acknowledgements The author would like to thank Mr. Morteza Yazdizadeh for helping to prepare samples.

Compliance with ethical standards

Conflict of interest The authors declare that they have no conflict of interest.

References

1. J.-Y. Dantan, Z. Huang, E. Goka, L. Homri, A. Etienne, N. Bonnet, M. Rivette, Geometrical variations management for additive manufactured product. *CIRP Ann.* **66**, 161–164 (2017). <https://doi.org/10.1016/j.cirp.2017.04.034>
2. C. Tan, K. Zhou, W. Ma, P. Zhang, M. Liu, T. Kuang, Microstructural evolution, nanoprecipitation behavior and mechanical properties of selective laser melted high-performance grade 300 maraging steel. *Mater. Des.* **134**, 23–34 (2017). <https://doi.org/10.1016/j.matdes.2017.08.026>
3. D. Ding, Z. Pan, D. Cuiuri, H. Li, Wire-feed additive manufacturing of metal components: technologies, developments and future interests. *Int. J. Adv. Manuf. Technol.* **81**, 465–481 (2015). <https://doi.org/10.1007/s00170-015-7077-3>
4. A. Ebrahimi, M. Mohammadi, Numerical tools to investigate mechanical and fatigue properties of additively manufactured MS1-H13 hybrid steels. *Addit. Manuf.* **23**, 381–393 (2018). <https://doi.org/10.1016/j.addma.2018.07.009>
5. Y. Nie, P. Zhang, X. Wu, G. Li, H. Yan, Z. Yu, Rapid prototyping of 4043 Al-alloy parts by cold metal transfer. *Sci. Technol. Weld. Join.* **23**, 527–535 (2018). <https://doi.org/10.1080/13621718.2018.1438236>
6. J.R. Hönnige, P.A. Colegrove, B. Ahmed, M.E. Fitzpatrick, S. Ganguly, T.L. Lee, S.W. Williams, Residual stress and texture control in Ti-6Al-4V wire + arc additively manufactured intersections by stress relief and rolling. *Mater. Des.* **150**, 193–205 (2018). <https://doi.org/10.1016/j.matdes.2018.03.065>

7. P.A. Colegrove, J. Donoghue, F. Martina, J. Gu, P. Prangnell, J. Hönnige, Application of bulk deformation methods for microstructural and material property improvement and residual stress and distortion control in additively manufactured components. *Scr. Mater.* **135**, 111–118 (2017). <https://doi.org/10.1016/j.scripamat.2016.10.031>
8. X. Xu, S. Ganguly, J. Ding, C.E. Seow, S. Williams, Enhancing mechanical properties of wire + arc additively manufactured INCONEL 718 superalloy through in-process thermomechanical processing. *Mater. Des.* **160**, 1042–1051 (2018). <https://doi.org/10.1016/j.matdes.2018.10.038>
9. Y. Guo, H. Pan, L. Ren, G. Quan, Microstructure and mechanical properties of wire arc additively manufactured AZ80M magnesium alloy. *Mater. Lett.* **247**, 4–6 (2019). <https://doi.org/10.1016/j.matlet.2019.03.063>
10. Y. Fu, H. Zhang, G. Wang, H. Wang, Investigation of mechanical properties for hybrid deposition and micro-rolling of bainite steel. *J. Mater. Process. Technol.* **250**, 220–227 (2017). <https://doi.org/10.1016/j.jmatprotec.2017.07.023>
11. Q. Wu, Z. Ma, G. Chen, C. Liu, D. Ma, S. Ma, Obtaining fine microstructure and unsupported overhangs by low heat input pulse arc additive manufacturing. *J. Manuf. Process.* **27**, 198–206 (2017). <https://doi.org/10.1016/j.jmapro.2017.05.004>
12. Y. Xie, H. Zhang, F. Zhou, Improvement in Geometrical Accuracy and Mechanical Property for Arc-Based Additive Manufacturing Using Metamorphic Rolling Mechanism. *J. Manuf. Sci. Eng.* **138**, 111002 (2016). <https://doi.org/10.1115/1.4032079>
13. H. Attar, M.J. Birmingham, S. Ehtemam-Haghighi, A. Dehghan-Manshadi, D. Kent, M.S. Dargusch, Evaluation of the mechanical and wear properties of titanium produced by three different additive manufacturing methods for biomedical application. *Mater. Sci. Eng. A.* **760**, 339–345 (2019). <https://doi.org/10.1016/j.msea.2019.06.024>
14. Y. Yang, Y. Zhu, M.M. Khonsari, H. Yang, Wear anisotropy of selective laser melted 316L stainless steel. *Wear* **428–429**, 376–386 (2019). <https://doi.org/10.1016/j.wear.2019.04.001>
15. O.O. Marenych, D. Ding, Z. Pan, A.G. Kostyrychev, H. Li, S. van Duin, Effect of chemical composition on microstructure, strength and wear resistance of wire deposited Ni–Cu alloys. *Addit. Manuf.* **24**, 30–36 (2018). <https://doi.org/10.1016/j.addma.2018.08.003>
16. A.S.T.M. International, G. ASTM, Standard Test Method for Wear Testing with a Pin-on-Disk Apparatus, ASTM Int. West Conshohocken, PA, USA. ASTM G99-0 (2016) 1–5. <https://doi.org/10.1520/G0099-05R10.2>
17. ASTM E384-99: Standard Test for Micro indentation Hardness of Materials, ASTM Int. West Conshohocken, PA, USA. (1999). <https://doi.org/10.1520/E0384-99>
18. American Society for Testing and Materials, ASTM A240: Standard Specification for Chromium and Chromium-Nickel Stainless Steel Plate, Sheet, and Strip for Pressure Vessels and for General Applications, ASTM Int. I (2004) 12. <https://doi.org/10.1520/A0240>
19. The international Nickel Company Inc, *Mechanical and Physical Properties of Austenitic Chromium-Nickel Stainless Steels at Ambient Temperatures*, 3rd edn. (INCO databooks, New York, 1968)
20. C.V. Haden, G. Zeng, F.M. Carter, C. Ruhl, B.A. Krick, D.G. Harlow, Wire and arc additive manufactured steel: Tensile and wear properties. *Addit. Manuf.* **16**, 115–123 (2017). <https://doi.org/10.1016/j.addma.2017.05.010>
21. J. Gu, J. Ding, S.W. Williams, H. Gu, J. Bai, Y. Zhai, P. Ma, The strengthening effect of inter-layer cold working and post-deposition heat treatment on the additively manufactured Al–6.3Cu alloy. *Mater. Sci. Eng. A.* **651**, 18–26 (2016). <https://doi.org/10.1016/j.msea.2015.10.101>
22. Z. Qi, B. Cong, B. Qi, H. Sun, G. Zhao, J. Ding, Microstructure and mechanical properties of double-wire + arc additively manufactured Al–Cu–Mg alloys. *J. Mater. Process. Technol.* **255**, 347–353 (2018). <https://doi.org/10.1016/j.jmatprotec.2017.12.019>
23. J. Gu, X. Wang, J. Bai, J. Ding, S. Williams, Y. Zhai, K. Liu, Deformation microstructures and strengthening mechanisms for the wire + arc additively manufactured Al–Mg4.5Mn alloy with inter-layer rolling. *Mater. Sci. Eng. A.* **712**, 292–301 (2018). <https://doi.org/10.1016/j.msea.2017.11.113>
24. F. Martina, S.W. Williams, P.A. Colegrove, Improved microstructure and increased mechanical properties of additive manufacture produced Ti–6Al–4V by interpass cold rolling, in: 24th Int. Free. Fabr. Symp. Austin, Texas, USA, 2013: pp. 490–496
25. H. Inoue, T. Koseki, S. Ohkita, M. Fujii, Formation mechanism of vermicular and lacy ferrite in austenitic stainless steel weld metals. *Sci. Technol. Weld. Join.* **5**, 385–396 (2000)
26. H. Inoue, T. Koseki, Clarification of solidification behaviors in austenitic stainless steels based on welding process. *Nippon Steel Tech. Rep.* **95**, 62–70 (2007). <http://www.nssmc.com/en/tech/report/nsc/pdf/n9511.pdf>
27. J. Elmer, S. Allen, T. Eagar, Microstructural development during solidification of stainless steel alloys. *Metall. Trans. A* **20**, 2117–2131 (1989). <https://doi.org/10.1007/BF02650298>
28. O. Yilmaz, A.A. Uгла, Microstructure characterization of SS308LSi components manufactured by GTAW-based additive manufacturing: shaped metal deposition using pulsed current arc. *Int. J. Adv. Manuf. Technol.* **89**, 13–25 (2017). <https://doi.org/10.1007/s00170-016-9053-y>
29. D.J. Kotecki, J.C. Lippold, *Welding metallurgy and weldability of stainless steels*, Wiley, Hoboken, NJ B. Barbero, E. Ureta Comp. Study Differ. Digit. Tech. Their Accuracy. *Comput Aided Des.* **43** (2005) 188–206
30. E. Ahmad, R. Priestner, Effect of rolling in the intercritical region on the tensile properties of dual-phase steel. *J. Mater. Eng. Perform.* **7**, 772–776 (1998). <https://doi.org/10.1361/105994998770347341>
31. M. Shunmugavel, A. Polishetty, G. Littlefair, Microstructure and mechanical properties of wrought and additive manufactured Ti–6Al–4V cylindrical bars. *Procedia Technol.* **20**, 231–236 (2015). <https://doi.org/10.1016/j.protcy.2015.07.037>
32. M.A. Maleque, M.S. Salit, *Materials Selection and Design* (Springer, Berlin, 2013)
33. P.K. Rai, S. Shekhar, K. Yagi, K. Ameyama, K. Mondal, Fretting wear mechanism for harmonic, non-harmonic and conventional 316L stainless steels. *Wear* **424–425**, 23–32 (2019). <https://doi.org/10.1016/j.wear.2019.02.005>
34. X. Cheng, Z. Jiang, D. Wei, H. Wu, L. Jiang, Adhesion, friction and wear analysis of a chromium oxide scale on a ferritic stainless steel. *Wear* **426–427**, 1212–1221 (2019). <https://doi.org/10.1016/j.wear.2019.01.045>
35. H. Li, M. Ramezani, M. Li, C. Ma, J. Wang, Tribological performance of selective laser melted 316L stainless steel. *Tribol. Int.* **128**, 121–129 (2018). <https://doi.org/10.1016/j.triboint.2018.07.021>
36. C. Palanisamy, S. Bhero, B. Abiodun Obadele, P.A. Olubambi, Effect of build direction on the microhardness and dry sliding wear behaviour of laser additive manufactured Ti–6Al–4V. *Mater. Today Proc.* **5**, 397–402 (2018). <https://doi.org/10.1016/j.matpr.2017.11.097>
37. D. Gu, C. Hong, G. Meng, Densification, Microstructure, and Wear Property of In Situ Titanium Nitride-Reinforced Titanium Silicide Matrix Composites Prepared by a Novel Selective Laser Melting Process. *Metall. Mater. Trans. A* **43**, 697–708 (2012). <https://doi.org/10.1007/s11661-011-0876-8>
38. X.-J. Shen, C. Zhang, Y.-G. Yang, L. Liu, On the microstructure, mechanical properties and wear resistance of an additively

- manufactured Ti64/metallic glass composite. *Addit. Manuf.* **25**, 499–510 (2019). <https://doi.org/10.1016/j.addma.2018.12.006>
39. H. Fu, Q. Xiao, H. Fu, Heat treatment of multi-element low alloy wear-resistant steel. *Mater. Sci. Eng. A.* **396**, 206–212 (2005). <https://doi.org/10.1016/j.msea.2005.01.023>
40. F. Wang, D. Qian, L. Hua, X. Lu, The effect of prior cold rolling on the carbide dissolution, precipitation and dry wear behaviors of M50 bearing steel. *Tribol. Int.* **132**, 253–264 (2019). <https://doi.org/10.1016/j.triboint.2018.12.031>

Publisher's Note Springer Nature remains neutral with regard to jurisdictional claims in published maps and institutional affiliations.